Chapter 7

Io's Extended Neutral Clouds

7.1   Introduction

The previous chapter discussed neutrals close to Io in the corona. The atoms in the corona are a mix of bound and escaping atoms ejected from Io's exobase. This chapter describes the atoms which escape from the corona; i.e., the atoms sputtered from Io's exobase with escape velocity. This represents the higher speed portion of the distribution, a sufficient number of atoms escape to make the extended and highly photogenic neutral clouds. Understanding the rate and directional distribution of the high speed portion of the sputtered velocity distribution provides details of the interaction between the plasma torus and Io's atmosphere: neutral cloud formation is a direct result of plasma bombardment at Io.

The model developed in Chapter 5 can address several questions regarding the neutral clouds and their changing morphology:

- What are the morphological features in the cloud and how are they explained through the motions of the neutrals?

- What are the significant differences between the sodium and oxygen cloud distributions?

- What effect does the torus have on the shape and extent of the cloud?

- What effect does the torus have on the emission from the oxygen cloud?

Understanding the origins of the morphological features and the complications associated with interpreting images and spectra of the extended neutral clouds are essential for determining the actual distributions of neutrals orbiting Jupiter. This chapter is therefore focused on answering these questions. Section 7.2 discusses the application of the model to the problem of the extended neutral cloud. I also describe the process of extracting measurable quantities from modeled images. In Section 7.3 I describe the morphological similarities and differences between the sodium and oxygen clouds. There are two types of differences: density differences which imply differences in the distributions of the atoms, and brightness differences which result from geometrical parameters specific to observations and peculiarities of the emission mechanisms. I also discuss the effect of the torus on the extent of the clouds. The next section introduces the sodium image archive containing over ten years of imaging data. These images will be essential for the future work with this model. The last section, Section 7.5 summarizes the results and includes a discussion of the joint analysis of the model and data.

7.2   Neutral Cloud Models

The workings of the neutral cloud model has already been described (Chapter 5): packets ejected from Io were tracked under the influence of gravity and lost by electron impact ionization and charge exchange in the plasma torus. Model images were created from the positions and un-ionized fractions of each packet. In Chapter 6, the model runs focused on the region within ~ 10 R_{Io} of Io as the area of interest was Io's corona. In this chapter, I concentrate on the extended neutral clouds of sodium and oxygen. Therefore, unless otherwise specified, all model images show the region within 10 R_J of Jupiter which includes Io's orbit and the outer edges of the neutral clouds. Models of the sodium cloud had a modeled duration of 50 hours, about 1-1/4 Io orbits around Jupiter. Because neutral oxygen has a significantly longer lifetime, the total time of

oxygen simulations was 200 hours. Other specific inputs to the model runs are discussed where appropriate.

The analysis of model images depended on the behavior or features being investigated with the model runs. Two basic methods were employed: (a) qualitative analysis of two-dimensional modeled images, and (b) radial decomposition of images into basic, measurable quantities.

Images of the neutral clouds from above Jupiter's north pole and as observed from Earth allow large structures to be examined (Figure 7.1). Images of this nature allow a qualitative comparison of the neutral clouds under different conditions. The view from above, not available to Earth-bound observers, helps describe the three-dimensional distribution of the neutral atoms. In addition to varying the viewing angle, several choices of the observed quantity are also available. The images in Figure 7.1 show the column density; it is also possible to form images in units of brightness (see Section 7.3.3 below). Column density images, although not of the observable quantities, are not dependent on the peculiarities of the different emission mechanisms. Images in brightness units are strongly dependent on the state of the plasma torus, in the case of oxygen, or the solar Fraunhofer lines, in the case of sodium.

A more quantitative analysis of the images is also possible by performing a radial decomposition to extract several basic quantities. This method allows model images to be compared to other models and provides quantities which can be extracted from images of the neutral clouds (see Section 7.4), making quantitative analysis of the neutral cloud in imaging data possible. The quantities peak intensity, direction, and width of the neutral cloud provide a simple way of describing the complex and asymmetric neutral clouds. Each quantity is measured as a function of distance from Io for the leading and/or trailing clouds. The peak intensity of the the cloud is defined as the maximum intensity along an arc with the constant radius r from Io. The direction is the angle along that arc from some reference point. I measure this angle clockwise from Jupiter
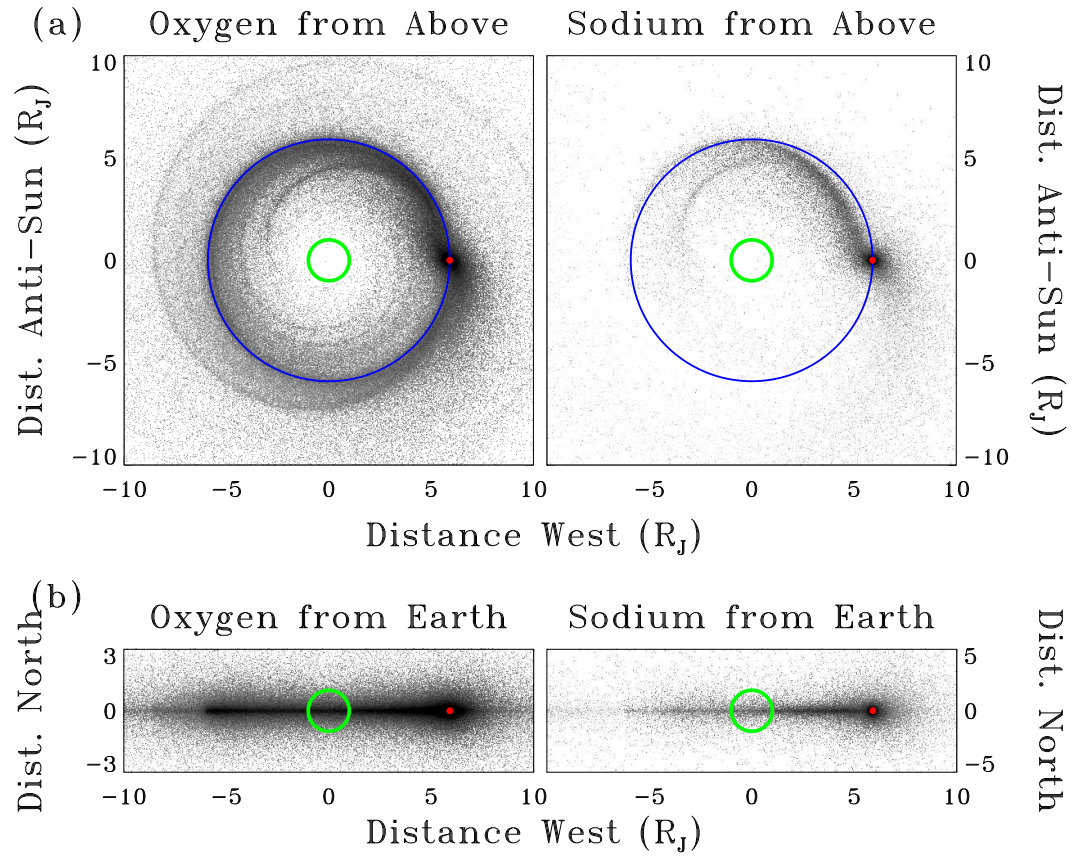
Figure 7.1 Examples of neutral clouds models. The left half shows the oxygen cloud column density from (a) above Jupiter's north pole and (b) Earth. Panels (c) and (d) show the sodium column density from above and Earth, respectively. The green circles indicate the location of Jupiter; the blue circles shows Io's orbit. Io is at western elongation.

north in model images unless otherwise specified. The width is the full width at half maximum measured in radians, for the angular width, or Jupiter radii, for the linear width, with $W_{Rj} = W_\theta r$.

To extract these values, the model images are binned into concentric rings about Io with each bin having a constant depth (dr) and width (dθ), both measured in Io radii (Figure 7.2). All the bins in an image have equal area; the number of bins in a ring increases as the distance form Io increases. Plots of an arc at a constant radius (Panel (c)) allow the location of the center of the cloud, the peak intensity of the cloud (Panel (d)), and the full width at half-maximum (FWHM, Panel (e)) to be measured. These quantities are then determined as a function of the distance from Io.

7.3   Large Scale Features

Examples of modeled clouds of oxygen and sodium are shown in Figure 7.1. The column densities are scaled relative to their source rates from Io's exobase; i.e., the greater column density of oxygen is a result of the difference in ionization rates of the two species, not their source rates. Several morphological features can be seen in these images; specifically, the leading sodium cloud interior to Io's orbit, the complete torus of neutral oxygen, and the sharp, well defined edges of the cloud. The following subsections contain discussions of these features and large scale differences between the sodium and oxygen clouds.

7.3.1   Motions of Neutral Atoms

Atoms ejected from Io in the forward direction make up the trailing cloud. These atoms have Io's velocity plus an added velocity which gives them more kinetic energy than Io and'orbits with greater semi-major axes. This causes them to move exterior to Io's orbit. As atoms move exterior to Io, they slow down relative to Io, which passes the atoms resulting in a trailing cloud (Figure 7.3). Conversely, atoms ejected in the
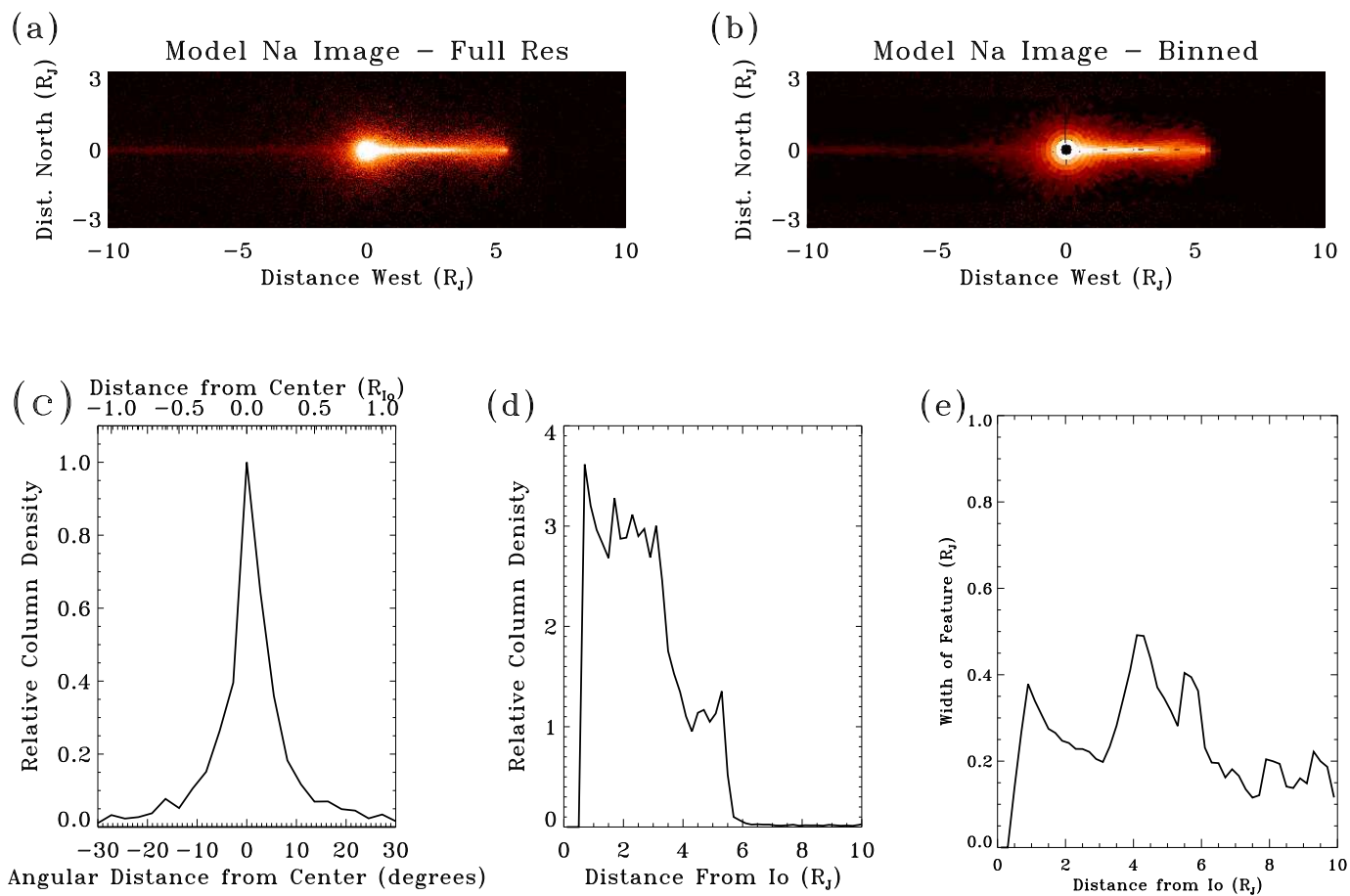
Figure 7.2 Decomposition of a model image into basic observable quantities. (a) Model image at full resolution. (b) Model image binned into concentric circles with each bin having a constant area. (c) Arc through the image at constant distance of 2.1 R_J from the center of Io. The angle and distance are measured clockwise from the center of the cloud. (d) Peak intensity versus distance from Io along the forward cloud. (e) Width of the cloud versus distance from Io along the forward cloud.

trailing direction have velocities slightly less than Io's orbital velocity and orbit Jupiter with smaller semi-major axes than Io. These atoms move interior to Io's orbit and will increase their velocities relative to Io forming a leading cloud.

The neutral cloud is composed of atoms with a distribution of initial velocities ejected into all directions. Therefore, understanding these images requires an understanding of how the initial velocity (both speed and direction) and initial location from the exobase affects the course of an atom. Streamlines for atoms as they travel from Io are given in Figure 7.4. In each panel the system is seen from above. Io is at western elongation, east is the negative x (left) direction and the sun is in the negative y (down) direction. The black circles show the location of Io's orbit. Each streamline shows the motion of the atoms relative to Io for 50 hours. Row (1) shows the initial locations and directions of each atom for the column that it heads: column (a) has atoms ejected from the sub-Jupiter point only; column (b) shows ejection from the leading point, column (c) from the anti-Jupiter point, and column (d) from the trailing point. Column (e) shows ejection from all four points together. The following rows each contain atoms ejected with a single velocity: 2.0 km s^{-1}, 2.5 km s^{-1}, 3.0 km s^{-1}, 3.5 km s^{-1}, 4.0 km s^{-1}, 5.0 km s^{-1}, 10.0 km s^{-1}, and 20 km s^{-1} in rows (2)-(9). The actual neutral cloud is made up of superpositions of streamlines of a distribution of velocities that is heavily weighted toward the low speed end of the distribution.

Row (2), which shows atoms with initial velocity 2 km s^{-1}, indicates that atoms with initial speeds less than the escape velocity from the exobase (2 km s^{-1}) contribute to the extended clouds. This is shown in detail in Figure 7.5. . The red streamlines are for the case when Io is a motionless body that is not immersed in Jupiter's gravitational field. In this case, none of the atoms escape from Io. They do, however, travel outside Io's Hill sphere, the effective limit of Io's gravitational domination, before turning around and heading back toward Io. The blue streamlines show the actual situation: Io is orbiting the large planet Jupiter. Under these circumstances, most atoms do escape.
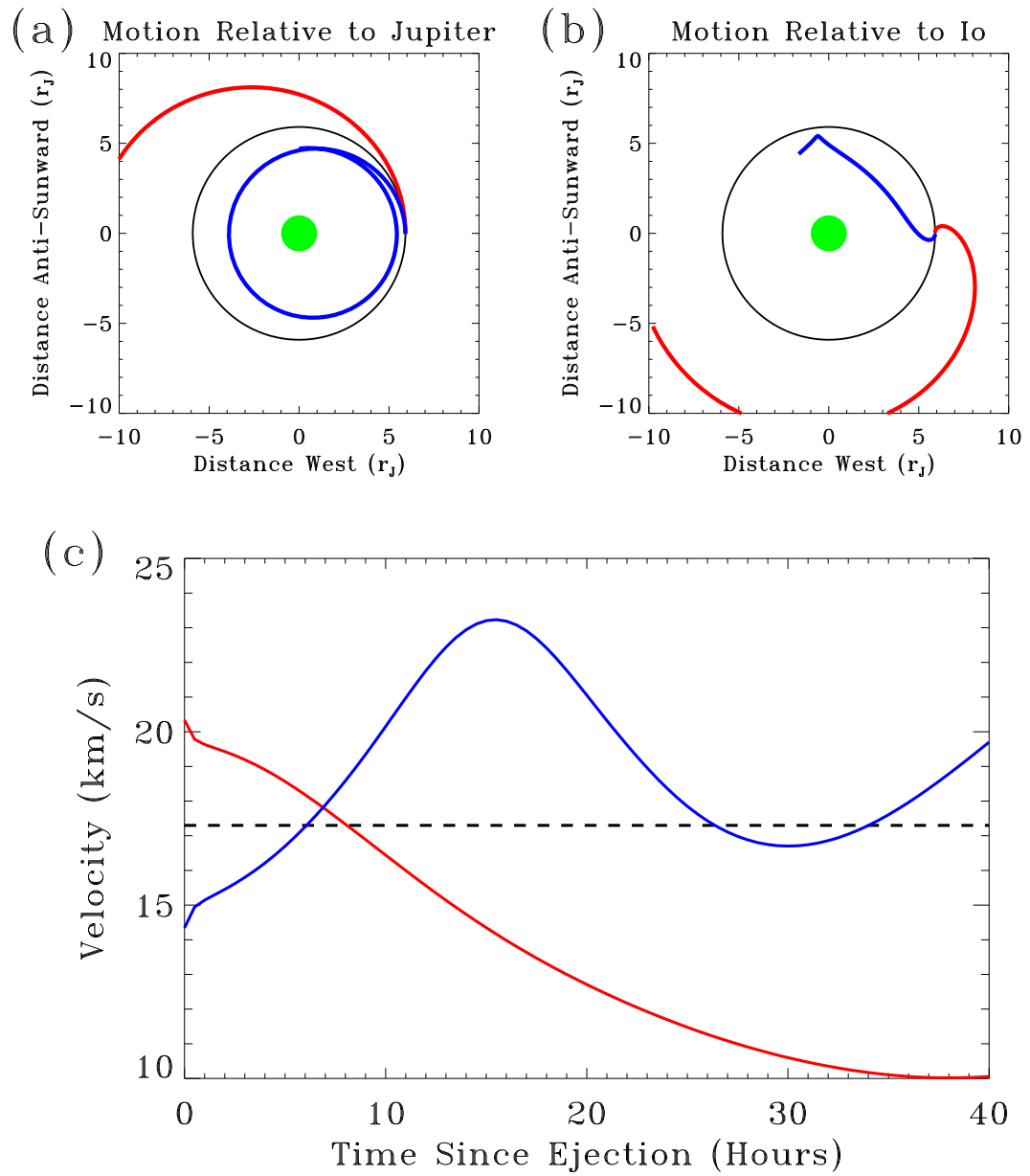
Figure 7.3 Sample trajectories of neutral atoms ejected from Io. The red path shows a sodium atom ejected in the direction of Io's motion; the blue path shows an atom ejected opposite to Io's motion. Both atoms have an initial velocity of 3 km s^{-1} relative to Io. The green filled circles show the location of Jupiter. Io is initially at western elongation; its orbit is shown by the black circle. Panel (a) shows the orbits of the atoms relative to Jupiter as seen from above. Panel (b) shows the motion of the atoms relative to Io. Panel (c) gives the velocity evolution of the atoms relative to Jupiter. The broken black line shows Io's constant orbital velocity.
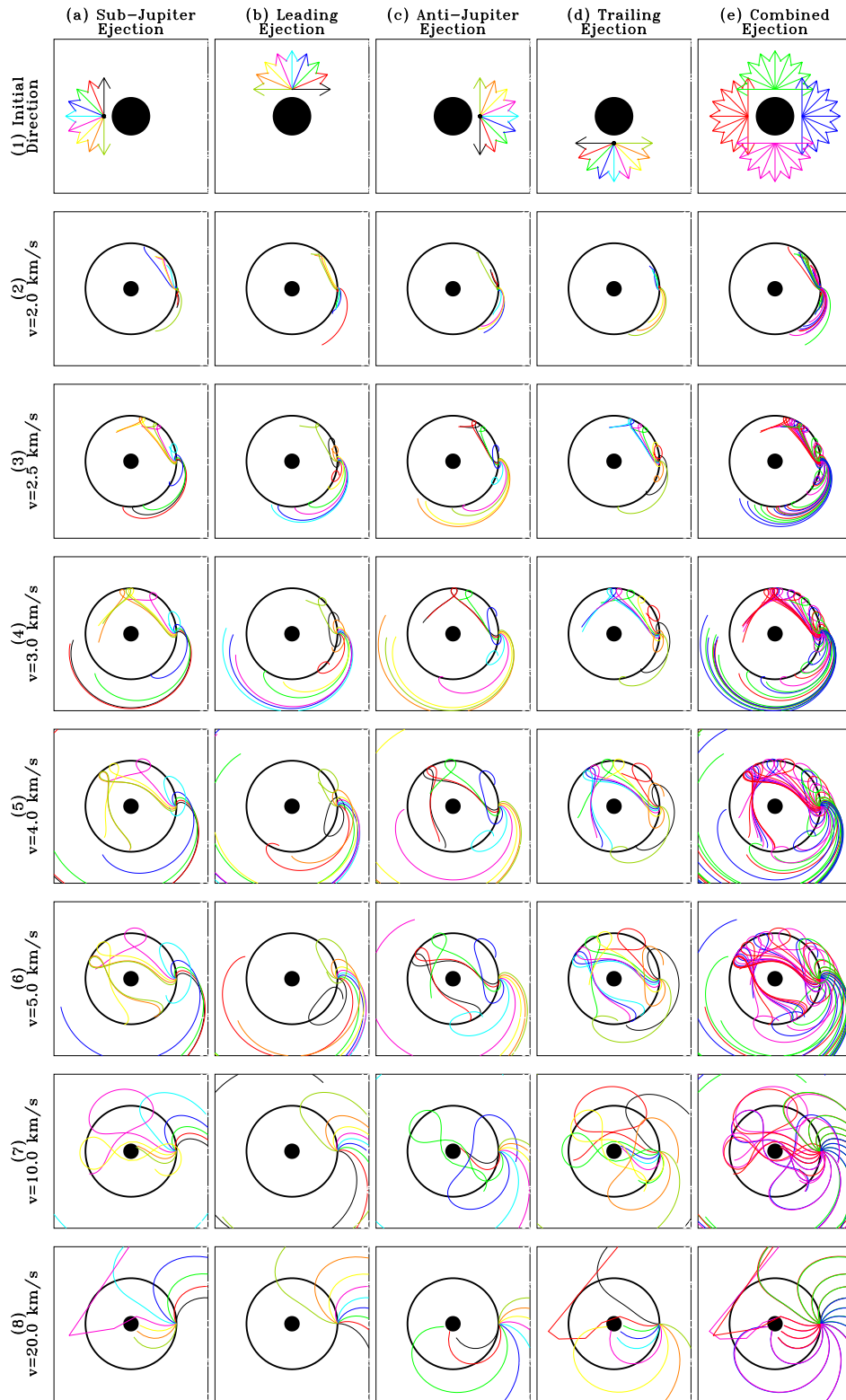
Figure 7.4 Streamlines of atoms ejected from Io with a range of speeds, directions, and location on Io's surface. See discussion in text.
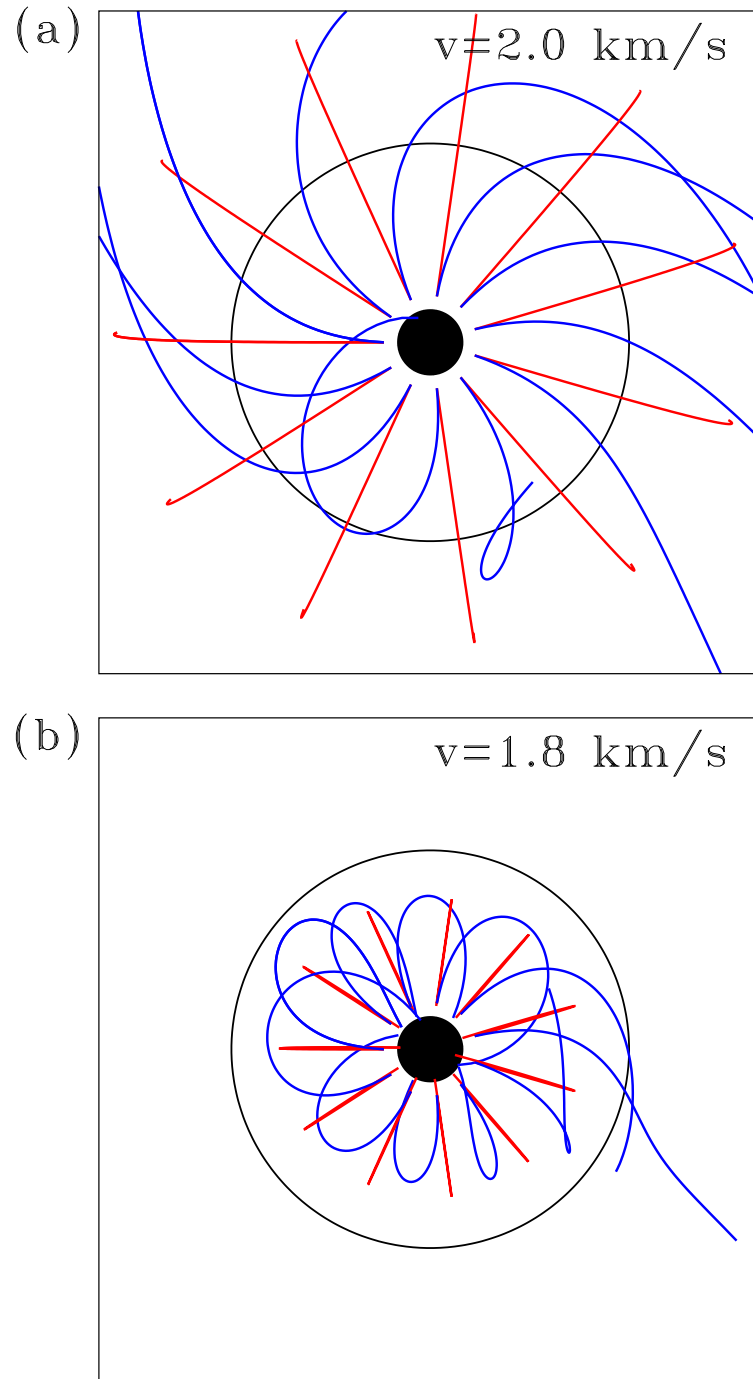
Figure 7.5 (a) Streamlines of atoms ejected from Io with initial velocity of 2 km s^{-1}. The red streamlines show the trajectories when Io is stationary and not immersed in Jupiter's gravitational field. The blue streamlines show their paths when Io is in motion around Jupiter. The black circle at 6 R$_{\text{Io}}$ shows the approximate location of Io's Hill sphere. (b) Same as (a) with initial velocity 1.8 km s^{-1}.
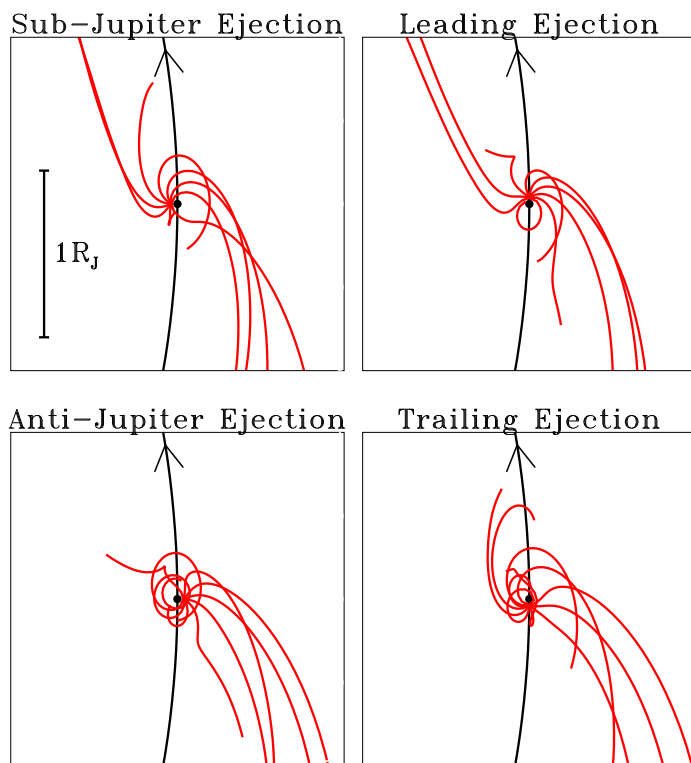
Those that do not are still strongly influenced by Jupiter's gravity: their trajectories are highly perturbed from the Jupiter-less case, but Io is still able to retain control. Panel (b) depicts the same situation for atoms which are not as close to the escape velocity. In this case, the atoms do not make it outside the Hill sphere and their motion is never dominated by Jupiter. The combination of Jupiter's gravity and Io's motion do perturb the streamlines, but in general all of the atoms are bound to Io. A few atoms do escape; conversely, some atoms ejected with greater than escape velocity will not escape.

Another important point is that atoms ejected from any location on the surface can contribute to both the leading and trailing clouds. Atoms with velocities greater than ~ 2.5 km s^{-1} are not greatly affected by Io's gravity as they escape the Hill sphere; therefore, the direction the atoms are ejected is the most important factor in determining which part of the extended cloud the atoms join. Atoms in these simulations are ejected isotropically over the hemisphere above each point on the exobase. From each point, some atoms will escape with velocities which puts them into the forward cloud and some with velocities which puts them into the trailing cloud. An intermediate scale view around Io is given in Figure 7.6 to show how atoms from different regions contribute to the extended clouds.

Some of the atoms do in fact hit Jupiter, in which case they are removed from the system. These are the atoms which are ejected in the trailing direction with speed ~ 17 km s^{-1}. An atom ejected with speed relative to Io that is equal to Io's orbital velocity but in the opposite direction has zero velocity relative to Jupiter and does not orbit; it falls. The atoms with greater speeds can go into retrograde orbit around Jupiter.

The leading cloud shows distinct inner and outer edges. The streamlines in Figures 7.4 and 7.6 help to shed light on the source of these boundaries. The outer edge occurs near Io's orbit at 5.91 R$_{\mathrm{J}}$. This is the apojove of the atoms interior to Io, creating an outer limit to the leading cloud. Because the atoms slow down as they approach

(a) Velocity = 2 km/s

Sub−Jupiter Ejection

Leading Ejection

Anti−Jupiter Ejection

Trailing Ejection

(b) Velocity = 3 km/s

Sub−Jupiter Ejection

Leading Ejection

Anti−Jupiter Ejection
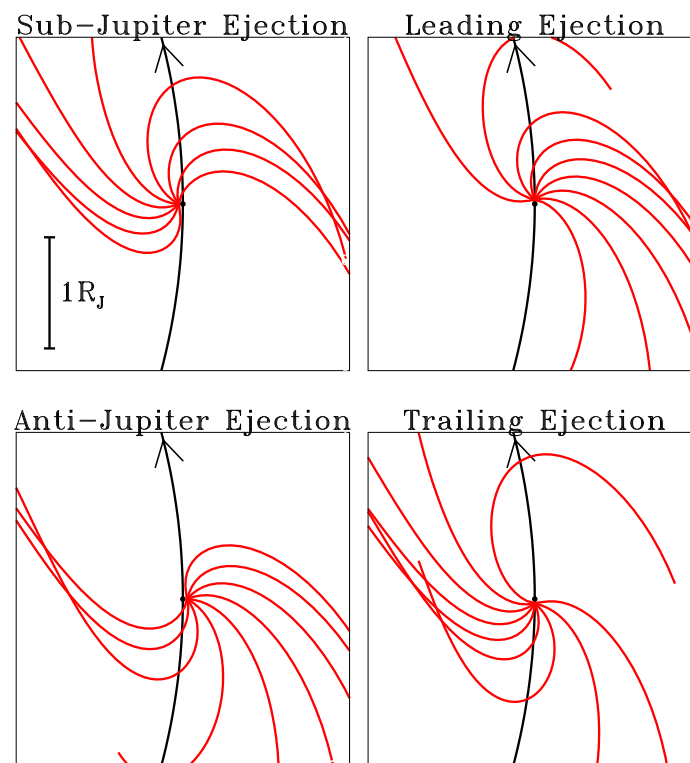

Trailing Ejection

Figure 7.6 Intermediate scale view showing streamlines of atoms from their escape to the exobase into the neutral clouds. In panel (a), all atoms are ejected with an initial velocity of 2 km s^{-1}. In panel (b) the initial velocity is 3 km s^{-1}. The four parts of each panel show escape from four locations on Io as indicated. The angle of escape is distributed over the hemisphere tangent to the surface at the point of escape. The scale of each panel is indicated: panel (a) is a 2 R$_J$ by 2 R$_J$ square centered on Io (shown to scale by the black filled circle) which is at western elongation, and panel (b) is a 3 R$_J$ by 3 R$_J$ square. Io's direction of motion is up in the image along its orbit (shown in black).

apojove, a density enhancement is created resulting in the brightening of the outer edge. The inner edge is due to the unequal distribution of streamlines in the leading cloud: ejection over a variety of angles leads to overlapping streamlines and an over-abundance of atoms in the inner edge. Column (e) if Figure 7.4 shows that for velocities between ~ 2 and 4 km s^{-1}, there are more streamlines at the inner edge of the cloud than the outer edge of the cloud creating the density enhancements seen in the model images. In the trailing cloud, the streamlines are more evenly distributed, so there are no density enhancements or sharp, well defined edges.

7.3.2   Loss of Neutral Atoms

Based on these motions, one might expect to see both leading and trailing clouds clouds around Io. Some of the earliest observations of sodium (e.g., Trafton and Macy (1975)), however, showed that the sodium cloud is predominantly a leading cloud: only the portion of the cloud leading Io in its orbit extends around Jupiter. Observations of the oxygen are more difficult, and therefore far fewer in number. The published observations of neutral oxygen outside the corona are inconclusive regarding the angular extent of the oxygen cloud. Brown (1981a) detected oxygen $\sim 180°$ away from Io, but could not determine from this observation if this emission was from the leading edge of the leading cloud or from a complete oxygen torus. More recent spectra (Thomas 1996) concentrated on the leading cloud and did not search for a trailing cloud.

The first attempts to understand the leading sodium cloud assumed non-isotropic ejection of sodium from Io since no mechanism for asymmetric loss was known. The discovery of the plasma torus provided such a mechanism (Trafton 1980; Smyth 1983). The first detailed treatment of the effect of the torus on the sodium lifetime was presented by Smyth and Combi (1988b). The structure of the plasma torus results in a highly non-uniform neutral lifetime. Sodium atoms in the leading cloud, which are interior to Io's orbit, lie mostly in the cold torus where electron temperatures are low and the

lifetime is long ($\gtrsim$ 7 hours within 5.7 R_J). The trailing cloud exterior to Io's orbit is in the warm torus, a region of higher electron temperature and shorter sodium lifetime ($\sim$ 3 hours) (Figure 7.7).

The circumstances are similar for oxygen: the neutral lifetime is shorter exterior to Io's orbit than interior. However, this lifetime is significantly longer: the minimum oxygen lifetime in the region near Io's orbit is $\sim$ 20 hours. The sodium lifetime is shorter than this everywhere outside 5.5 R_J from Jupiter. Therefore, ionization does not provide such a stringent limit on the size of the cloud and a complete neutral oxygen torus forms rather than a banana-shaped leading cloud. The portion of the cloud trailing Io is made up of atoms ejected in the forward direction which then lag behind Io in its orbit. Because the oxygen lifetime in the warm torus is much longer than the sodium lifetime, oxygen atoms survive long enough to form this additional portion of the neutral clouds. Sodium is ionized too quickly to allow a trailing cloud to be sustained.

7.3.3   Neutral Cloud Brightnesses

The previous sections concern the motions and ionization of neutral atoms and the implications on the column densities of these species. However, remote observations of the neutral clouds are made of line emission brightnesses; column densities must be inferred from the emissions. Figure 7.8 shows brightnesses for the model simulations for which column densities were given in Figure 7.1. The most obvious difference between these figures is that while the oxygen column density is greater and the cloud is more extensive than sodium, its brightness is much less. In this section I discuss some of the some of the factors which must be considered when examining observations. For sodium, the main factors are the effect of the solar Fraunhofer line and the changing viewing geometry from Earth. As oxygen atoms depend on the plasma to excite the emitting electrons, the instantaneous state of the plasma has the greatest effect on the intensity.
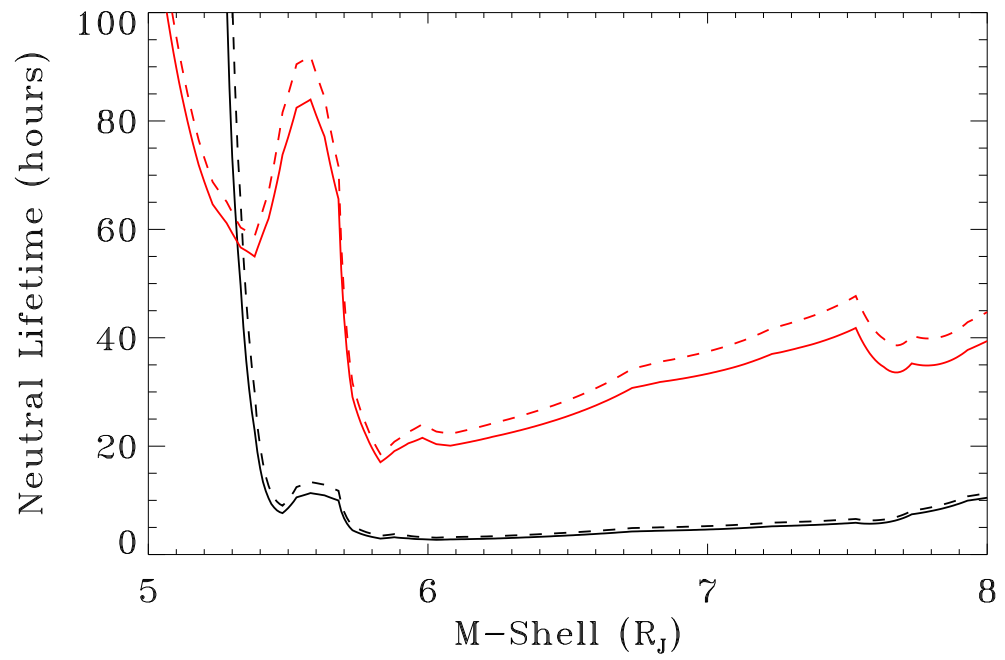
Figure 7.7 Average neutral lifetimes of sodium (black) and oxygen (red) in the torus as function of the modified L-shell parameter M. The solid lines are the lifetimes at western elongation and the broken lines are the lifetimes at eastern elongation.
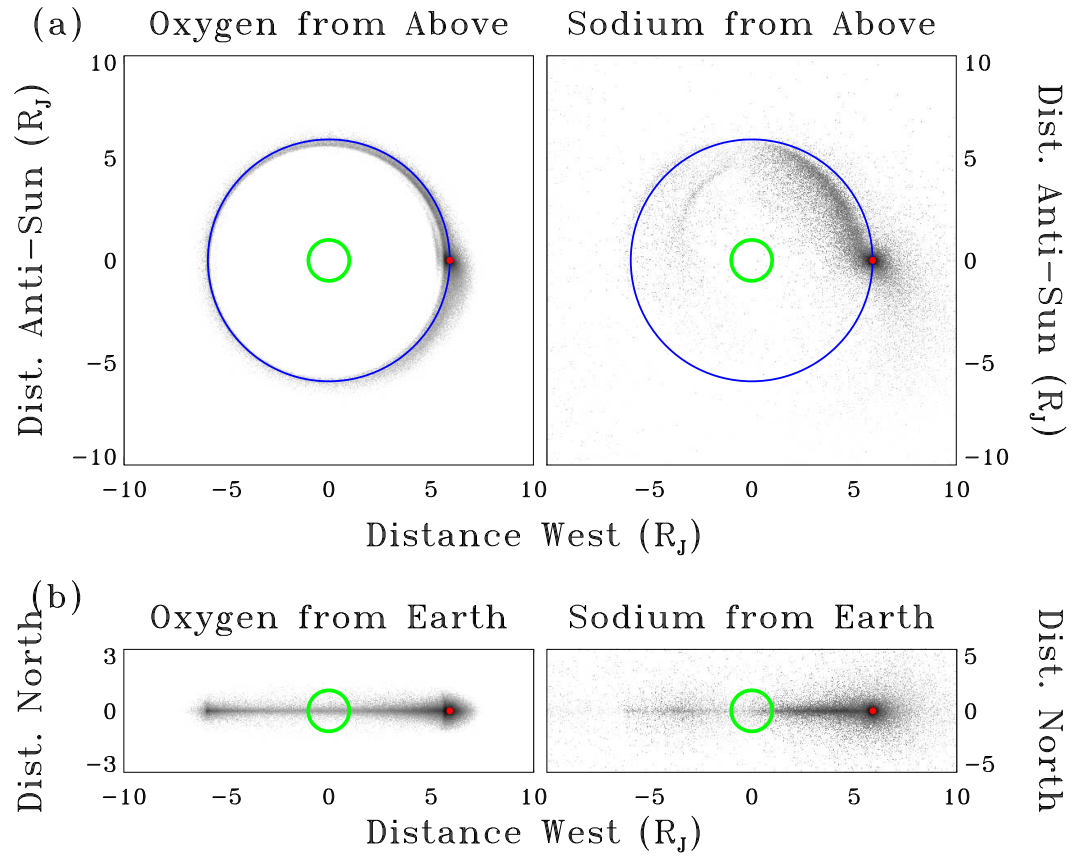
Figure 7.8 Examples of modeled neutral cloud brightnesses. The images were created from the same model runs as the column density images in Figure 7.1.

Factors Affecting Observed Sodium Brightnesses

Io's motion and the motions of the atoms in the cloud result in large variations in sodium intensity which must be understood to determine which brightness variations imply actual changes in the densities of neutral atoms that result from changes in the source or loss rates. Here I will discuss several effects related to the importance of radial velocity relative to the sun and viewing geometry of the sodium cloud on the observed brightness.

The largest factor on the observed intensity and morphology of the neutral cloud far from Io is the changing geometry from which the cloud is viewed as Io orbits Jupiter. Because the cloud is banana shaped and extends along Io's orbit, it looks very different when Io is in front of Jupiter, so that the cloud is seen along its side, than when Io is nearing elongation and the cloud is seen roughly head on. Figure 7.9 shows the cloud as seen at several orbital longitudes assuming it is static as Io moves around Jupiter from superior heliocentric conjunction to eastern elongation. The variations in morphology are due entirely to Io's orbital motion and not any sodium density differences. As can be seen, the brightness of the cloud is extremely variable, but should not be confused with real variations in the distribution of neutrals relative to Io. All the visible changes are due to factors which do not affect the cloud itself, just how the cloud is illuminated and viewed.

Close to Io, the sodium brightness is dominated by Io's changing radial velocity relative to the sun. The deep solar sodium D Fraunhofer lines result from absorption by sodium atoms in the sun's atmosphere. The width of these lines are greater than the range of the Doppler shift of Io caused by Io's motion around Jupiter, implying that sodium near Io never experiences the full brightness of the solar continuum. Because of the steep profiles of the Fraunhofer lines (Figure 1.2), the fraction of the solar intensity available to Io (the γ-factor in Equation 2.9) is a strong function of Io's orbital phase. Figure 7.10 shows how the intensity of sodium in the region near Io (i.e., in the corona)
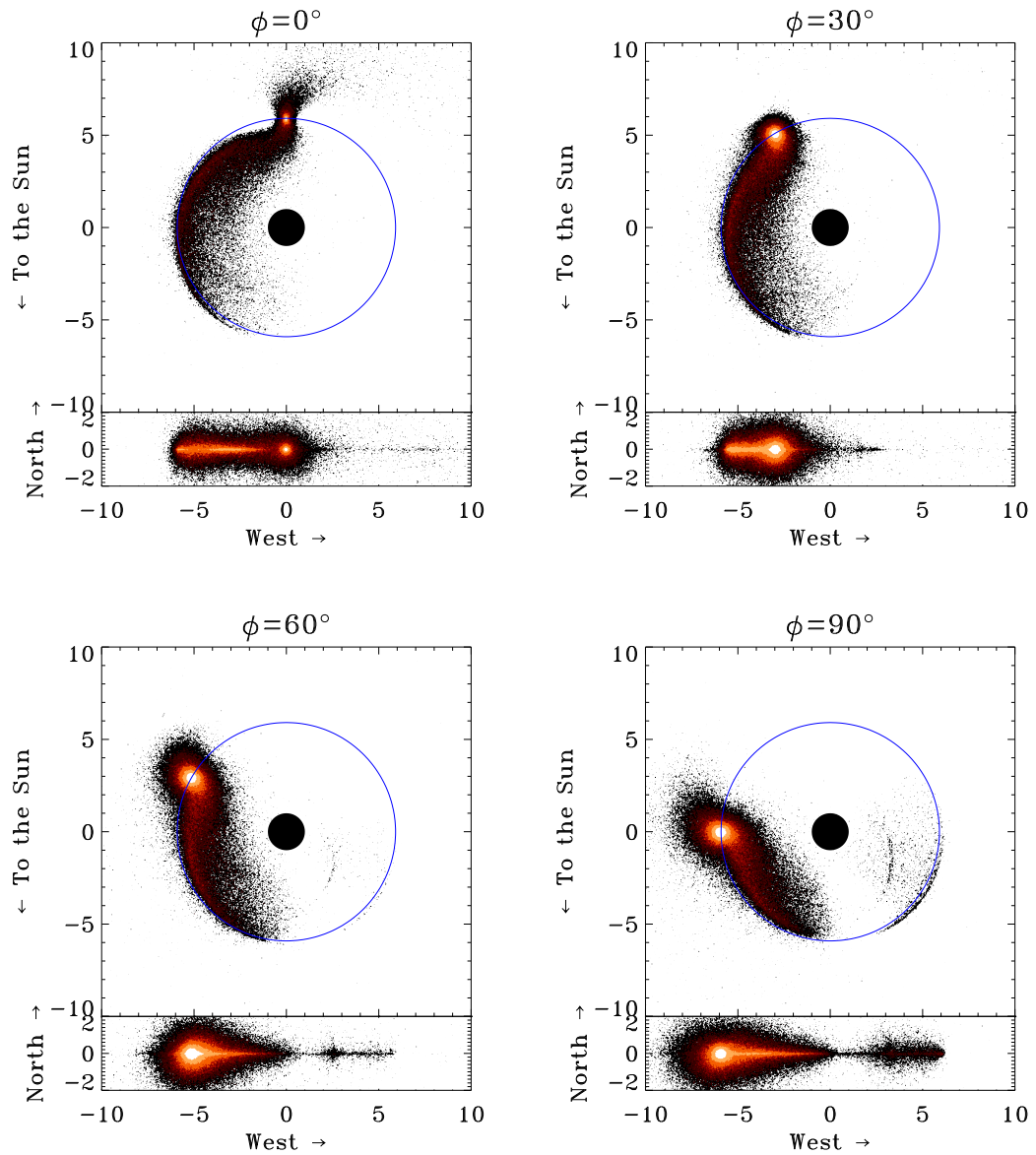
Figure 7.9 The series of images show Io at four orbital phases keeping the sodium cloud densities constant. The Jupiter system is seen from above and from Earth at each location. All differences in morphology are due to the changing viewing geometry and the effects of resonant scattering in the deep solar Fraunhofer lines.
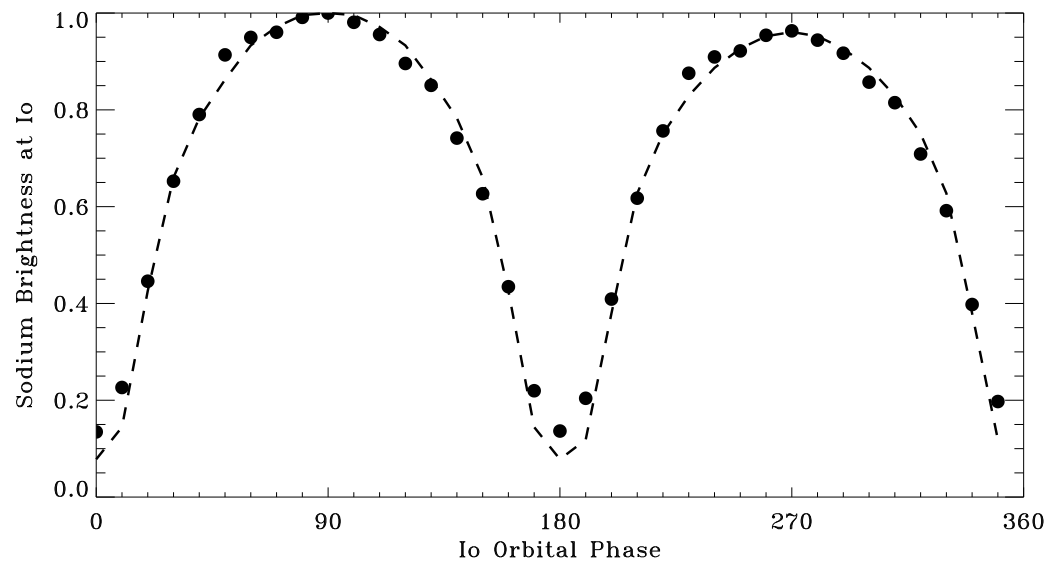
Figure 7.10 Intensity of sodium in Io's corona as a function of orbital phase assuming a static sodium distribution as Io orbits Jupiter. The broken line shows the expected variation in intensity based solely on the changing γ-factor. The intensity is normalized to the brightness at eastern elongation.

varies as Io orbits Jupiter, again assuming that the sodium distribution around Io remains constant. The circles show the relative modeled brightness at Io; over-plotted is the predicted intensity variation based on the changing value of γ. When Io's radial velocity relative to the sun is zero, the intensity of the sodium cloud at Io is $\sim 10\%$ of its peak brightness. Of course, Io cannot be observed at these orbital phases since Jupiter is either blocking Io ($\phi \sim 0°$) or many orders of magnitude brighter ($\phi \sim 180°$), but even for geometries where Io is visible there is a significant change in brightness. The early observations of Io's sodium intensity (Bergstralh et al. 1975; Trafton and Macy 1975) detected these variations as a function of orbital phase and provided the proof that the emission mechanism is resonant scattering. The slight east/west asymmetry in Figure 7.10 stems from an asymmetry in the D_2 Fraunhofer line. The magnitude of this asymmetry is smaller than the observed the east/west asymmetry which is due to asymmetries in the neutral lifetime and represents a physical difference in the corona (Smyth and Combi (1988b) and see Chapter 6).

The large variations in γ also have a significant effect on the the brightness profile of the cloud along its length (Figure 7.11). The column density of sodium along the cloud when Io is at western elongation decreases at a slower rate than the brightness profile because the latter profile combines the effects of the changing density and changing radial velocity. Toward the leading edge of the cloud, the intensity increases despite the fact that the column density is still decreasing. This is because the radial velocity, and therefore γ, is increasing faster than the column density decreases. The rate at which column density decreases slows as the cloud approaches eastern elongation since the cloud turns along the observer's line-of-sight. The cloud brightness however primarily increases due to the additional factor of increasing γ as the radial velocity of sodium increases. The magnitude of this effect is greatest in front of or behind Jupiter where the cloud cannot be observed. However it is important to distinguish which brightening effects on the opposite side of Jupiter from the cloud are due to column density increases
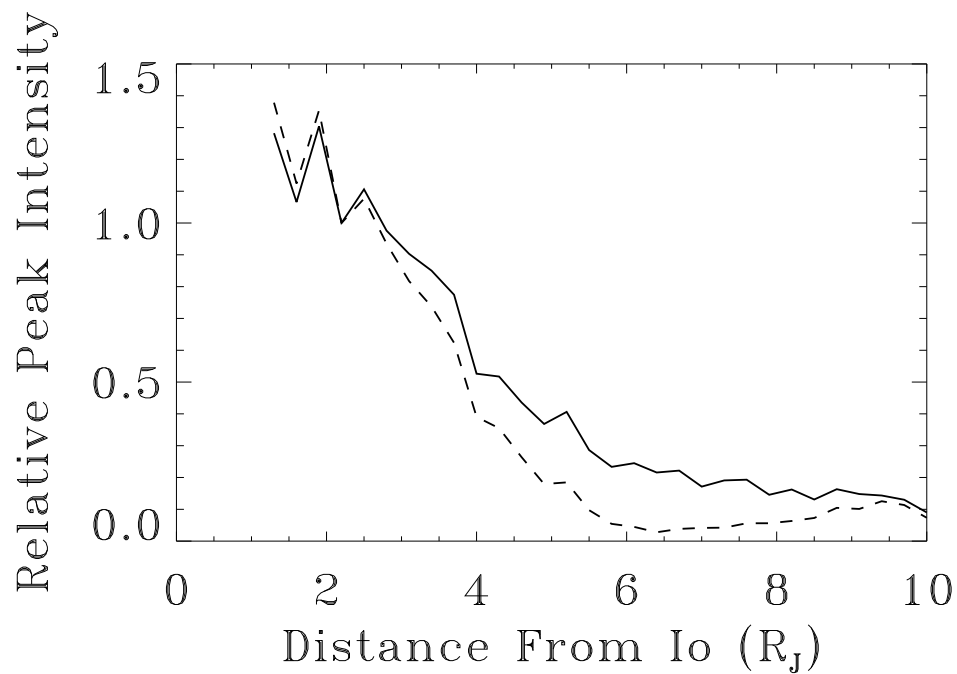
Figure 7.11 A comparison of the column density profile (solid line) and brightness profile (broken line) for the sodium cloud image shown if Figure 7.1. The curves are normalized to unity at 2 R_J from Io. The brightness profile decreases at a faster rate than the column density profile due to the changing value of γ.

along the line-of-sight and which are due to the increasing radial velocity.

A smaller factor also must be considered when comparing the models with data: the angle relative to Io's orbital plane at which Earth-based observers view the sodium cloud varies over the course of Jupiter's twelve year orbit. When comparing images separated by several years, the difference in the sub-Earth latitude of the observer on Jupiter becomes important. Although the emission by sodium and oxygen is isotropic, and is not affected by the direction from which the observations are made, the lines of sight do change and effects the perceived cloud morphology. Figure 7.12 show an example of how the sub-Earth latitude affects the view of the sodium cloud. The effects are most prominent near Io where the densities are the largest. Similarly, phase angle variations over the course of a year change the sight-lines through the cloud and the measured brightnesses.

Factors Affecting Oxygen Brightness

The brightest emission line of neutral oxygen at visible wavelengths ([OI]6300 Å) is excited by electron impacts. Therefore, the intensity of the emission is highly dependent on the state of the plasma torus. Figure 7.13 shows a series of model images of the oxygen cloud where the only parameter which changes between images is Io's magnetic longitude. The shapes and peak intensities of the cloud at greatest elongation from Jupiter are highly variable as a function of the torus orientation (Figure 7.14).

Because the oxygen intensity is such a strong function of the local plasma conditions, it is very difficult to extract the oxygen column density from emission intensity without knowing the state of the plasma torus. The variation in the brightness of the cloud at maximum eastern elongation from Jupiter as several torus parameters vary is shown in Figure 7.14. In the model run from which these images were created, Io is at western elongation, so the intensities are measured 180° away from Io.

Panel (a) shows the variation with magnetic longitude both with and without the effects of the observed System-III variation in the torus. The effect of System-III
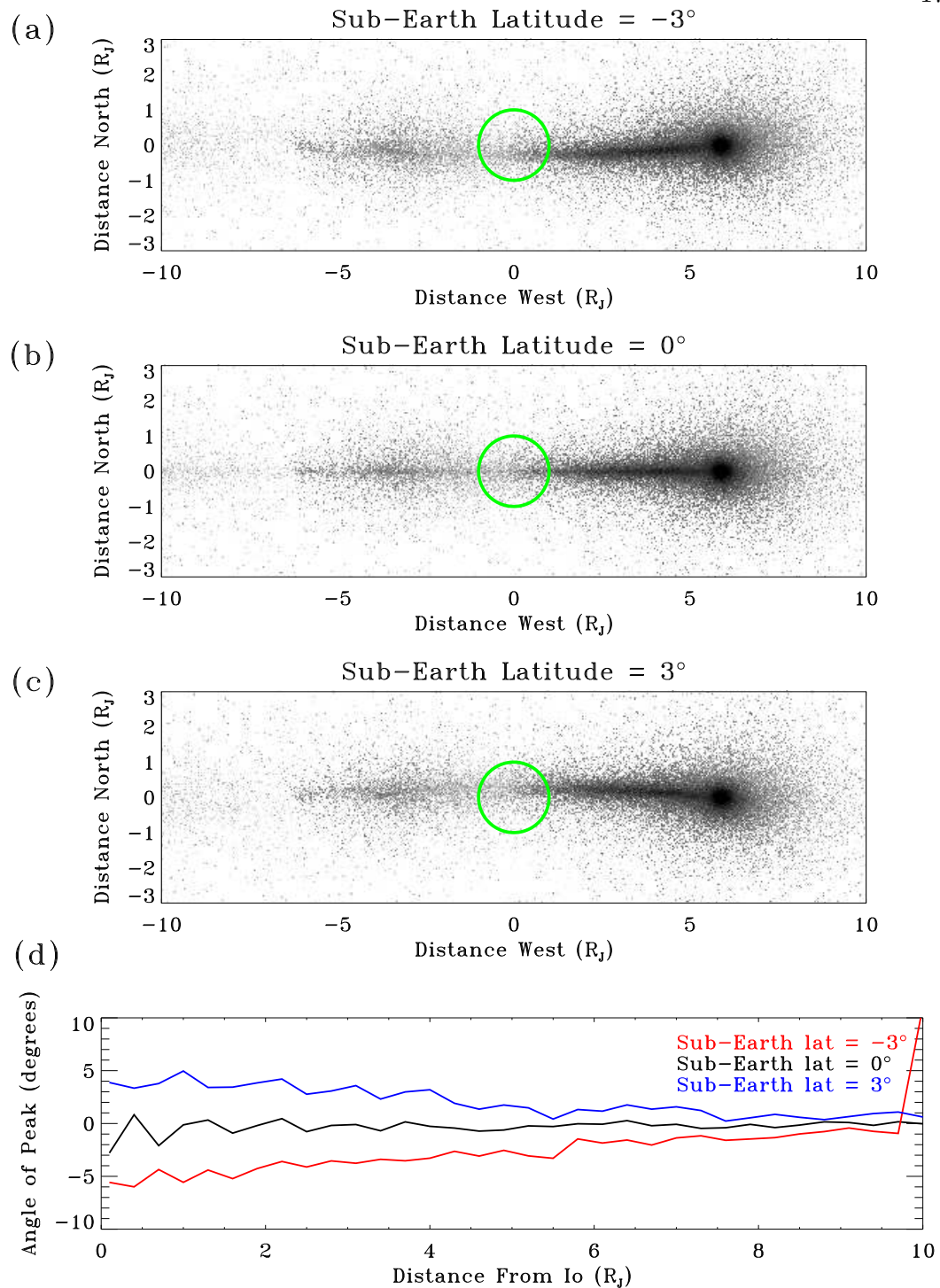
Figure 7.12 The effect of the tilt of Jupiter's equatorial plane relative to Earth. Panel (a) shows the appearance of the cloud when Jupiter's north pole is tilted 3° away from the observer, panel (b) shows no tilt, and panel (c) shows the cloud with Jupiter tilted 3° toward Earth. The green circles show the location of Jupiter in the image. Io is at western elongation. Panel (d) gives the angle of the peak intensity relative to Io's orbital plane for each image. The angle is measured clockwise from East: positive angles indicate that the cloud is rotated north, negative angles are south of the plane.

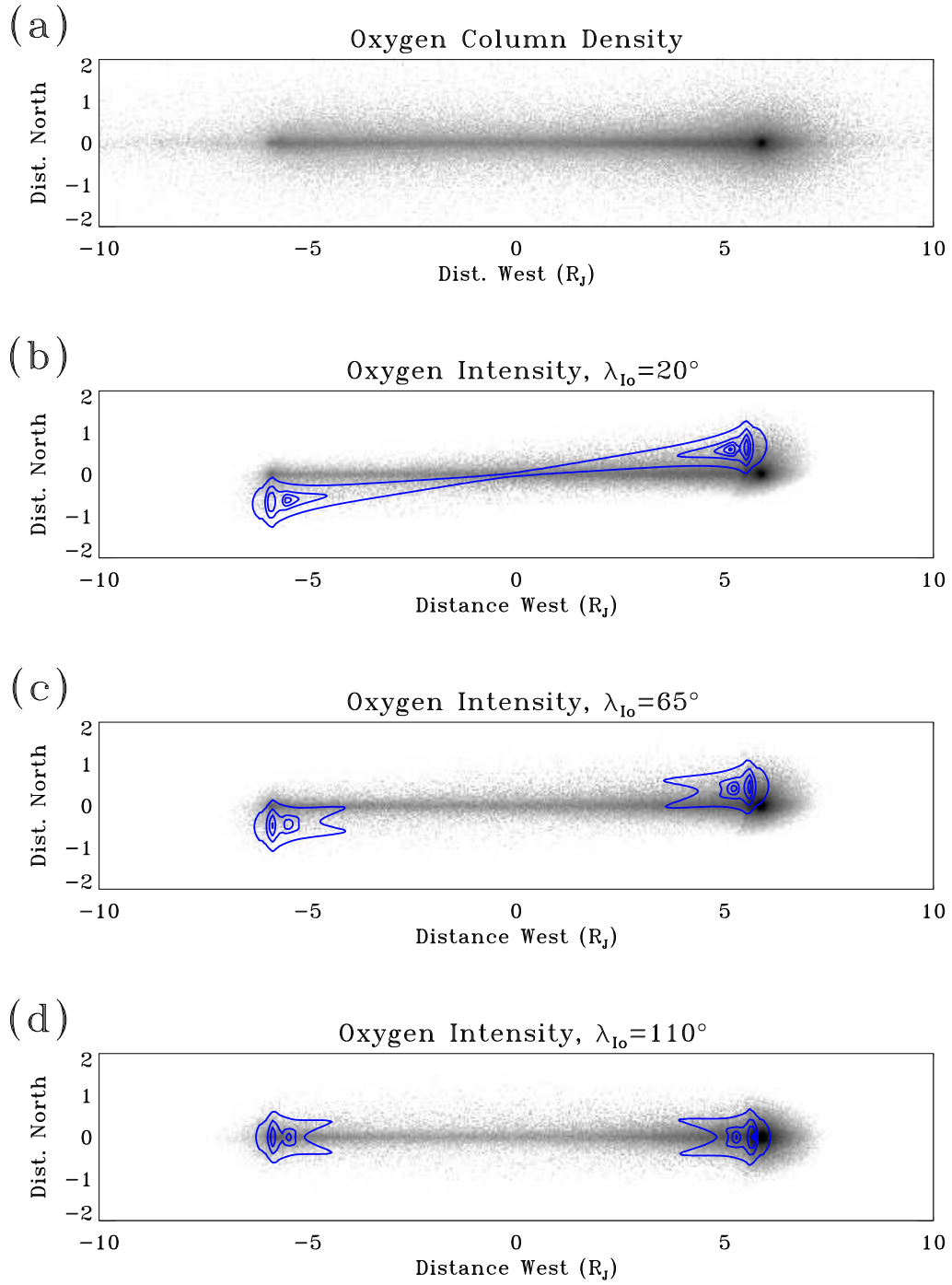Figure 7.13 (a) Model image showing column density of oxygen as observed from Earth. Io is at western elongation. (b) [OI] 6300 Å brightness for the image in (a) for $\lambda_{Io} = 20°$. The orientation of the plasma torus is shown in blue. (c) Brightness for $\lambda_{Io} = 65°$. (d) Brightness for $\lambda_{Io} = 110°$.
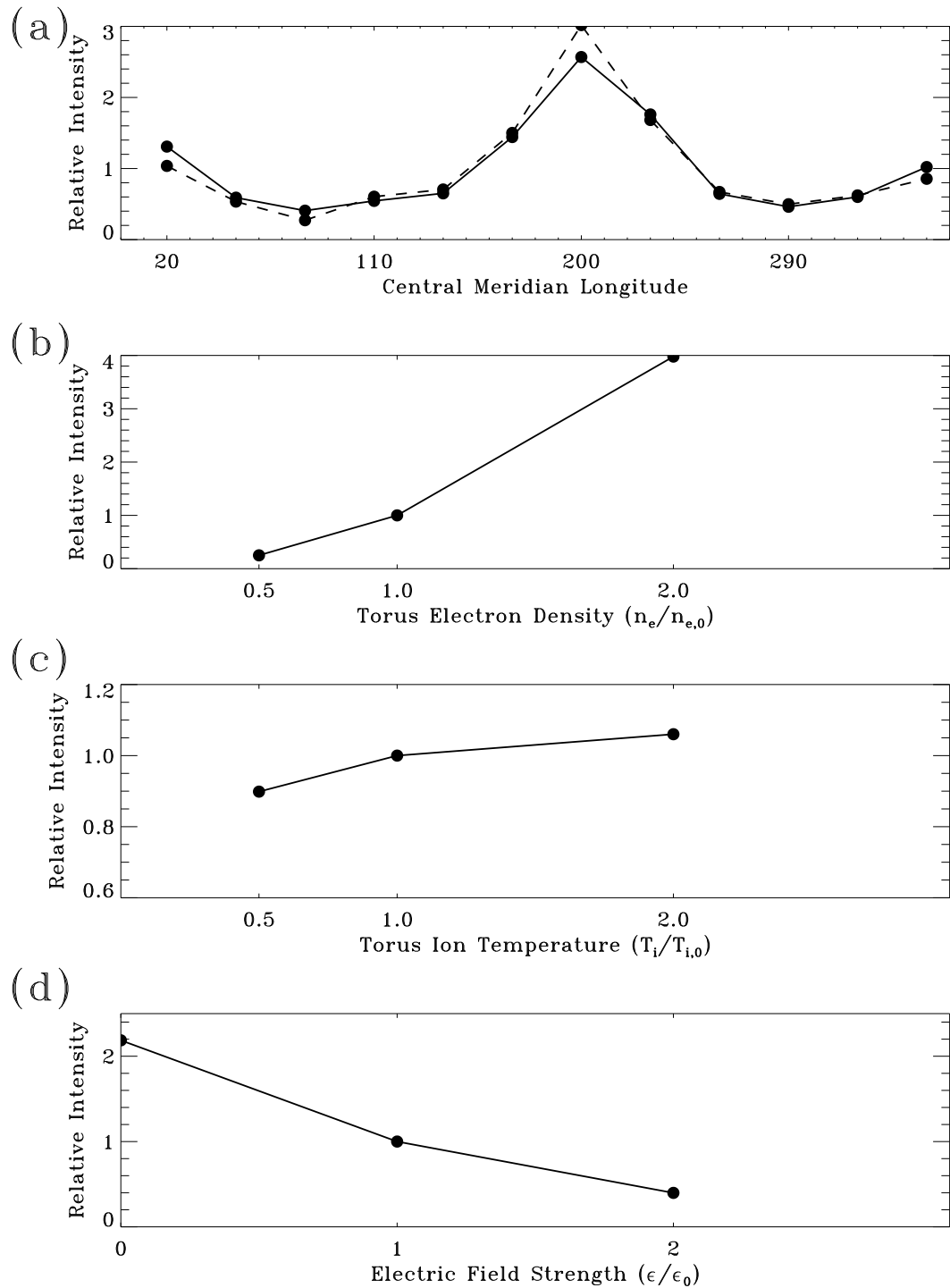
Figure 7.14 Variation in oxygen cloud brightness 180° from Io due to torus variability. Io is at western elongation; brightnesses are measured at eastern elongation at the distance of Io's orbit. (a) Intensity versus CML. The solid line is for a torus has no magnetic longitude variation; the broken line includes the observed variation. (b) Intensity versus torus electron density measured relative to the observed Voyager electron densities. (c) Intensity versus torus ion temperature. (d) Intensity versus east/west electric field strength.

variations are a second order effect on the brightness: the torus geometry is the main factor which determines the brightness. The offset and tilt of the centrifugal equator from the center of Jupiter introduces extreme variability in the intensity despite the fact that the density of oxygen in these images remains constant. Because the magnetic longitude of the observed region is known, it is possible to account for these effects and to coordinate observations with the times of maximum expected emission. Because the System-III variations in the torus have a relatively small effect on the intensity, the uncertainties introduced by this unknown variable are small compared to uncertainties in the overall torus densities and temperatures.

Changes in electron density in the torus (panel (b)) introduce large variability into the oxygen cloud. The emission rate is proportional to the product of the electron density and the emission rate coefficient, which is itself a function of electron density. The result is that relatively small changes in the electron density produce significant changes in intensity. Because the magnitude of the east/west electric field determines the shift of the torus to the east and the amplitude of local time variations in the torus, the intensity is also a strong function of the field strength (panel (d)).

If the electron density and temperature, ion temperature, field strength, and the magnitude of any System-III variability are not known, uncertainties in the column density of oxygen could be as high as an order of magnitude. Therefore determining the densities of oxygen far from Io and using these densities to determine the characteristics of the escape from Io is an uncertain proposition. Observations of oxygen should ideally be coupled with observations of the torus which can determine at least some of these varying parameters so as to reduce the uncertainty in interpreting the oxygen column densities.

7.4   Observations of the Sodium Neutral Cloud

Between 1990 and 2000 a series of observations of neutral sodium and singly ionized sulfur were made from the University of Arizona Catalina Observatory 1.5 meter telescope. Between 1990 and 1994, the JPL Coronographic Imager described by Schneider and Trauger (1995) was used. The second set of observations started in 1999 with the LPL coronograph (Hansell et al. 1995) adapted to observations of Io. Table 7.1 summarizes the observing runs which contributed to the image archive, many of which will be useful for future work on the neutral clouds.

Although the two sets of sodium images from Catalina Observatory used different instruments, the observing techniques were similar. The instruments use coronographic optics to reduce Jupiter's intensity and eliminate (or at least minimize) the spikes from Jupiter and the Galilean satellites caused by diffraction off the edges of the secondary mirror and its supports (Lyot 1939). Removing the diffraction features is essential for these observations because the large diffraction spikes off Jupiter in particular can hinder the analysis by obscuring the interesting sodium features. Coronographs also provide easy access to the telescope's focal plane. When observing the solar corona, an occulting spot is placed over the sun's disk to observe the much fainter corona. For observations of the inner Jovian system, a neutral density filter is used to cover Jupiter, reducing the planet's intensity by $\sim 10^{-3} - 10^{-4}$ without eliminating it from the images completely. Because Jupiter's intensity is known, it can be used as a standard calibration source present in each image as long as the neutral density filter is calibrated by comparing images of Jupiter with and without the filter in place.

The images were recorded by a CCD which changed between observing runs. The exposure times varied between 120 and 600 seconds. The standard observing strategy was to alternate between exposures through a narrow-band (~ 15 Å) sodium interference filter centered near 5889 Å and a narrow band interference filter centered on the 6716 Å

Date	Orbital Coverage	Magnetic Coverage	Number of Images	Lead Observer
10 Jan 1990	$136° - 206°$	$314° - 185°$	11	Schneider
11 Jan 1990	$334° - 55°$	$241° - 150°$	9	Schneider
12 Jan 1990	$174° - 257°$	$177° - 89°$	27	Schneider
7 Feb 1990	$92° - 134°$	$323° - 100°$	13	Schneider
8 Feb 1990	$270° - 292°$	$185° - 257°$	6	Schneider
10 Feb 1990	$314° - 23°$	$70° - 296°$	24	Schneider
30 Jan 1991	$24° - 41°$	$281° - 337°$	5	Schneider
31 Jan 1991	$170° - 247°$	$38° - 293°$	8	Schneider
1 Feb 1991	$16° - 52°$	$355° - 111°$	10	Schneider
2 Feb 1991	$217° - 280°$	$293° - 140°$	8	Schneider
4 Feb 1991	$260° - 338°$	$173° - 69°$	7	Schneider
5 Feb 1991	$100° - 100°$	$109° - 109°$	1	Schneider
6 Feb 1991	$305° - 338°$	$60° - 169°$	8	Schneider
21 Feb 1991	$126° - 191°$	$9° - 219°$	10	Schneider
22 Feb 1991	$323° - 34°$	$293° - 164°$	22	Schneider
23 Feb 1991	$221° - 221°$	$58° - 58°$	1	Schneider
24 Feb 1991	$64° - 71°$	$4° - 25°$	2	Schneider
25 Feb 1991	$207° - 220°$	$113° - 155°$	5	Schneider
26 Feb 1991	$69° - 75°$	$120° - 139°$	3	Schneider
5 Feb 1992	$232° - 264°$	$34° - 140°$	8	Schneider
9 Feb 1992	$309° - 352°$	$125° - 266°$	4	Schneider
26 Mar 1992	$289° - 339°$	$125° - 290°$	6	Schneider
30 Mar 1992	$23° - 70°$	$273° - 67°$	9	Schneider
31 Mar 1992	$228° - 234°$	$222° - 244°$	2	Schneider
10 Feb 1993	$74° - 80°$	$124° - 141°$	3	Schneider
14 Feb 1993	$175° - 175°$	$293° - 293°$	1	Schneider
24 Jul 1994	$30° - 36°$	$98° - 118°$	3	Schneider
25 Jul 1994	$219° - 49°$	$356° - 258°$	6	Schneider
26 Jul 1994	$52° - 248°$	$270° - 193°$	10	Schneider
27 Jul 1994	$255° - 89°$	$215° - 131°$	11	Schneider
28 Jul 1994	$101° - 127°$	$171° - 255°$	6	Schneider
30 Jul 1994	$148° - 174°$	$66° - 151°$	5	Schneider
11 Oct 1999	$151° - 216°$	$57° - 270°$	34	Burger
12 Oct 1999	$352° - 54°$	$354° - 200°$	32	Burger
29 Nov 1999	$18° - 87°$	$244° - 110°$	34	Burger
30 Nov 1999	$225° - 279°$	$202° - 19°$	25	Burger
23 Sep 2000	$36° - 67°$	$89° - 190°$	8	Burger
24 Sep 2000	$249° - 277°$	$68° - 159°$	9	Burger
25 Sep 2000	$80° - 121°$	$334° - 108°$	12	Burger
27 Dec 2000	$245° - 312°$	$292° - 152°$	14	Burger
28 Dec 2000	$87° - 152°$	$235° - 85°$	20	Burger
29 Dec 2000	$289° - 357°$	$176° - 39°$	22	Burger
30 Dec 2000	$131° - 196°$	$116° - 331°$	18	Burger

Table 7.1 Summary of all available sodium images

or 6731 Å line of [SII]. These near simultaneous images of Io's neutral sodium features and the plasma torus can be used to look for simultaneous changes in the neutral and plasma environments. In general, the fields of view of the images are large enough to contain the entire inner Jovian system (~ 10 R_J east and west of Jupiter). Therefore, all the sodium features encircling Jupiter were observed, not simply the sodium near Io. The large field of view in these images has previously been used with great success by Schneider et al. (1991b) who discovered the molecular ion stream on the opposite side of Jupiter from Io. It was also possible to observe both the east and west ansae of the plasma torus simultaneously (Schneider and Trauger 1995). These conclusions drawn from these torus images were used in Chapter 5 to describe the local time and magnetic longitude variations in the plasma torus.

Quantitative measurements of the sodium cloud are difficult since the cloud is not necessarily symmetric and there no obvious shapes to compare with. The basic quantities used to describe the images are the as as those discussed above to describe the models. The method for extracting these quantities was the same as for extracting them from models although the the background subtraction in the images was often not perfectly accomplished, requiring lines to be fit to the background regions of the arc.

7.5   Summary

This chapter describes the basic modeling results of the extended neutral oxygen and sodium clouds. I also discussed many of the difficulties associated with interpreting images and spectra of these species related to the changing viewing geometry, effects of radial motion relative to the sun, and the influence of the plasma torus on the oxygen emission. In addition, the major features in the column density structure were described in terms of the motions of neutral atoms escaping from Io and the ionization of these atoms by the plasma torus.

I also introduced the archive of available sodium images from the Catalina Obser-

vatory which extends back to 1990. Between 1990 and 1994, Schneider et al. obtained data with the JPL Coronographic Imager; in 1999 and 2000, I used the LPL Corono-graph to extend this data set. Because the near-simultaneous images were taken of the neutral sodium cloud and the sulfur plasma torus, it will be possible to use this data set in conjunction with the model to better constrain both the variability in the plasma torus and the influence of the plasma torus on the sodium cloud.